Microporous and Mesoporous Materials 359 (2023) 112647

Contents lists available at ScienceDirect

Microporous and Mesoporous Materials

journal homepage: www.elsevier.com/locate/micromeso

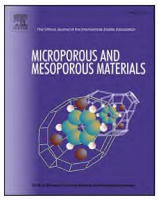

In vivo and *in vitro* studies of efficient mephedrone adsorption over zirconium-based metal-organic frameworks corroborated by DFT+D modeling

Przemysław J. Jodłowski [a,*], Klaudia Dymek [a], Grzegorz Kurowski [a], Kornelia Hyjek [a], Anna Boguszewska-Czubara [b], Barbara Budzyńska [c], Anna Pajdak [d], Łukasz Kuterasiński [e], Witold Piskorz [f], Piotr Jeleń [g], Maciej Sitarz [g]

[a] *Faculty of Chemical Engineering and Technology, Cracow University of Technology, 24 Warszawska, 31-155, Kraków, Poland*
[b] *Department of Medical Chemistry, 4A Chodzki, Medical University of Lublin, 20-093, Lublin, Poland*
[c] *Independent Laboratory of Behavioral Studies, 4A Chodzki, Medical University of Lublin, 20-093, Lublin, Poland*
[d] *Strata Mechanics Research Institute of the Polish Academy of Sciences, Reymonta 27, 30-059, Kraków, Poland*
[e] *Jerzy Haber Institute of Catalysis and Surface Chemistry, Polish Academy of Sciences, Niezapominajek 8, 30-239, Kraków, Poland*
[f] *Faculty of Chemistry, Jagiellonian University, Gronostajowa 2, 30-387, Kraków, Poland*
[g] *Faculty of Materials Science and Ceramics, AGH University of Science and Technology, Mickiewicza 30, 30-059, Kraków, Poland*

ARTICLE INFO

Keywords:
Metal-organic frameworks
Mephedrone
Adsorption
Behavioral studies
DFT

ABSTRACT

Mephedrone (4-MMC), due to its psychoactive effects similar to amphetamines and cocaine, and much lower price, is currently one of the most abused drugs by adolescents. Due to its commonness and low price, it is one of the stimulants that causes a strong mental and physical addiction, even leading to overdosing or the occurrence of strong withdrawal effects. In this work, we describe comprehensive spectroscopic and biomedical research on zirconium-based metal-organic frameworks (MOFs) for efficient, yet gradual, 4-MMC removal. Several methods including FTIR, μRaman, ^{1}H NMR, UV–Vis, and DFT were used to characterize the 4-MMC adsorption on MOFs. It was found that due to the structural similarities of both 4-MMC and MOF, spectroscopic signals overlap and the use of combined techniques such as DR UV–Vis/dissolution ^{1}H NMR may be required to comprehensively characterize 4-MMC adsorption. According to the 4-MMC adsorption tests, the adsorption efficiency as well as its kinetics strongly depends on the MOF structure parameters. The maximum 4-MMC adsorption from 1000 μM *aq.* Solutions were achieved by NU-1000 reaching *ca.* 45 wt% of adsorption. Additionally, by using the modulated synthesis of UiO-$66_{25\%\ HCl}$ with hydrochloric acid, 4-MMC adsorption efficiency increases from 24 wt% to 35 wt %. The *in vitro* and *in vivo* experiments have confirmed that the addition of MOF to the 4-MMC solutions decreases the 4-MMC concentration allowing proper *Danio rerio* embryo development. Furthermore, the *in vivo* experiments proved that MOFs are potentially safe for model organisms. Additionally, the *in vivo* experiments have proven the cardioprotective properties of MOFs.

1. Introduction

Among many psychoactive substances, legal highs and "club drugs" keep gaining more and more popularity among young people. Their availability, price, and legal loopholes make them more and more easily available and thus cause numerous health and social problems. According to the European Monitoring Centre for Drugs and Drug Addiction, every year 50 newly reported psychoactive substances are reported [1]. The drug black market in the EU is estimated to be worth about 24 billion each year [2]. According to the recent report by the European Monitoring Centre for Drugs and Drug Addiction (EMCDDA), the European market is dominated by cannabis (38%), heroin (28%), and cocaine (24%) without taking into consideration the amounts of so-called "legal highs" or "new psychoactive substances" (NPS) which are not on the list of illegal substances due to their fast synthesis and wide distribution. It is estimated that every week about 2 new psychoactive substances are introduced into circulation, which constitutes 8% of drug use among adolescents [2]. Difficulties related to the detection of

* Corresponding author.
E-mail address: przemyslaw.jodlowski@pk.edu.pl (P.J. Jodłowski).

https://doi.org/10.1016/j.micromeso.2023.112647
Received 16 February 2023; Received in revised form 21 April 2023; Accepted 14 May 2023
Available online 15 May 2023

NPS in the environment and the ease of distribution of precursors for their production make them widely available on the black market as well as on Darknet. The effective prevention and monitoring of illicit drugs are challenging since drug use usually takes place in drug undergrounds, closed events, or private homes. The recent report on drug abuse at Glastonbury Festival 2019 showed that the problem of drug abuse not only has a negative impact on human health and life but also has a negative effect on fauna [3]. During the Glastonbury Festival in 2019, increased drug content downstream of Whitelake River reached maximum concentrations equal to 32.33 ng/L, 548.41 ng/L, and 322.77 ng/L for cocaine, benzoylecgonine, and MDMA, respectively. The high cocaine concentration in the Whitelake River resulted in the disruption of European eels' endocrine system which hypothetically caused the extinction of this species.

The problem of drug abuse is not limited to annual rock festivals but occurs globally. In Table 1 the occurrence of the most popular illicit drugs was summarised based on monitoring of drug abuse based on measuring drugs and/or drug metabolites in urban wastewater. The method called sewage-based epidemiology (SBE) allows for the accurate determination of drug concentration based on drug metabolites from untreated urbane wastewater [4]. The analysis of the data shown in Table 1 illustrates the wide spectrum of illicit drugs that were detected in urban wastewater. In Europe, high concentrations of such drugs as mephedrone (4-MMC), amphetamine, methamphetamine, cocaine, and MDMA were recently detected. It is worth mentioning that the problem of water pollution is not limited to the psychoactive compounds in Table 1, but also includes other compounds such as methcathinone, butylone, and isomers (1-(2-methoxyphenyl)piperazine, 1-(4-methoxyphenyl)piperazine; 1-(2-flurophenyl)piperazine, 1-(4-flurophenyl) piperazine; 1-(3-trifluoromethylphenyl)piperazine, 1-(4-trifluoromethylphenyl)piperazine) [5], methylenedioxypyrovalerone (MDPV), benzylpiperazine (BZP), trifluoromethylphenylpiperazine (TFMPP), and 1-(3-chlorophenyl)piperazine (mCPP) [6] and many others.

The presence of drugs in domestic sewages that end up in wastewater treatment plants is an enormous challenge from a technological point of view due to the fact that standard wastewater treatment procedures are not fully efficient in the case of drug-contaminated water. As previously reported in work by Haalck et al. [7] the removal efficiency (RE%) of illicit drugs in wastewater treatment plants (WWTPs), the complete removal using standard WWTPs cleaning methods was achieved only for amphetamine (100 RE%), and nearly 100 RE% for benzoylecgonine and cocaine (94 and 98 RE% in WWTPs in Uppsala, 98 and 99 RE% in WWTPs in Stockholm, respectively). The removal efficiency for other illicit drugs like MDMA or methamphetamine, the RE%, was equal to 26 and 64 RE% in WWTPs in Uppsala and 21 and 37 RE% in WWTPs in Stockholm, respectively. More importantly, the negative RE% was observed for ketamine and 4-MMC reaching −28 and −31 RE% in WWTPs in Uppsala. The negative RE% indicates that higher amounts of drugs were detected after the wastewater treatment process which was probably due to the biodegradation of precursors in sewage or post-treatment re-partitioning of drug metabolites to the processed sewage. The problem of drug removal during the wastewater treatment becomes acute when comparing the amounts of 4-MMC and ketamine in Bologna and Cambridge where the maximum measured concentrations of those drugs were equal to 24 ng/L and 57.8 ng/L (Bologna) and $5.49{\cdot}10^5$ ng/L and $9.72{\cdot}10^4$ ng/L (Cambridgeshire wastewater), respectively.

Among the numerous drugs of abuse, mephedrone ((RS)-2-methylamino-1-(4-methylphenyl)propan-1-one, 4-MMC) among the others have a high priority on detection and development of the methods for removal from wastewater or human detoxification due to the fact that it is the most recreationally abused drug around the world. Due to its similar effects to amphetamine, MDMA, or cocaine, low price, easy accessibility, and high purity, it has been a predominant drug of abuse in seizures. Until the 4-MMC was listed as an illegal substance, it was widely available in drug markets, "legal high" shops, the internet, and even gas stations [8]. Despite its banning in most countries in 2010 [9], its popularity was still growing resulting in an increase in the death rate of drug addicts. In addition to its wide popularity among the youth, 4-MMC is gaining popularity among the clubbers and so-called "chemsex". The trend of the "*chemsex*" abbreviated from the term "sex under the influence" is rapidly growing mainly within the group LGBT and refers to the use of the drug of abuse like mephedrone, MDMA, and amphetamine in the presence of cocaine, ketamine, GHB and/or alcohol ("date-rape drug") to enhance the sensations during sexual intercourse [10]. The combination of multi-drug abuse has been reported as responsible for serious health problems or deaths [9–11].

Taking all the above-mentioned issues related to the removal of illicit drugs from urban wastewater it may be concluded that there is an urgent need to develop novel and efficient methods for the removal of illicit drugs which could be characterized as efficient, reliable, and safe for living organisms.

The recent developments in the synthesis and application of metal-organic frameworks (MOF) as adsorbents make them good candidates for the application to the removal of illicit drugs during wastewater treatment. Since the MOFs have been first been announced to the research community in the early '90s [12], numerous literature reports on their successful use in various applications including catalysis [13–15], energy storage [16], adsorption [17,18], drug delivery [19,20] and medicine [21,22]. The remarkable success of the application of MOFs for adsorption purposes triggered increased research into their use for the adsorption of hazardous materials from water. The wide range of possible applications of MOFs for the removal of hazardous materials includes the removal of hazardous dyes [23], herbicides/pesticides in groundwater [24,25], hazardous organics [26], heavy metals [27], and radionuclides [28]. Among the many possible applications of MOFs, their possible application for the adsorption of hazardous materials from aqueous media is currently under intense investigation. The main lines of research focus on the adsorptive removal of pharmaceutical drugs and personal care products (PPCPs) that are instantly produced and released to the environment from hospitals and households. Several studies on

Table 1
The concentrations of illicit drugs in wastewater samples worldwide.

Area	Highest compound concentration, [ng/L]						
	4-MMC	AMPH	METH	MDMA	COC	KET	Ref.
WWTP[a], Kraków, Poland	42.9	–	–	40.9	–	–	[80]
WWTP[a], Poznań, Poland	8.9	139.9[b]	–	51.8	–	–	[4]
Redlake River, USA	–	–	–	322.77	32.33	–	[3]
Beiyunhe River, China	–	11.3	92.2	–	10.7	–	[81]
Bologna, Italy	24	–	–	–	–	54.8	[82]
Cambridge, United Kingdom	$5.49{\cdot}10^5$	$2.30{\cdot}10^4$	$7.15{\cdot}10^4$	–	–	$9.72{\cdot}10^4$	[5]

[a] WWTP- wastewater treatment plant.
[b] Determined from amphetamine metabolites; 4-MMC-mephedrone; MC-methcathinone; AMPH-amphetamine; METH-methamphetamine; MDMA-methylenedioxymethamphetamine (ecstasy); COC- cocaine; KET-ketamine.

the efficient removal of such contaminants as diclofenac sodium (DCF), chlorpromazine hydrochloride (CLF), amodiaquine dihydrochloride (ADQ) [29], ibuprofen and acetaminophen [30], methotrexate [31], and many others [32].

Among the numerous synthesised MOFs presented in the literature, zirconium-based MOFs are under intense investigation due to their high thermal and chemical stability, high biocompatibility, and low cytotoxicity properties [33–35]. The previous successful application of UiO-66 and NU-1000 for medical purposes, especially as drug carriers [36,37] and adsorbents of hazardous compounds like uremic toxins [18] made them a natural choice in the search for potential NPS adsorbents. The selected for this study MOFs are composed of Zr_6-oxo-clusters connected by terephthalate ligands for UiO-66 [38] and 1,3,6,8-tetrakis (p-benzoate)pyrene ($TBAPy^{4-}$) for NU-1000. The differences between organic linkers in both Zr-based MOFs result in different topologies and porous characteristics of UiO-66 and NU-1000) (Fig. 1). The UiO-66 topology may be summarised by the formula $[Zr_6(\mu_3\text{-}O)_4(\mu_3\text{-}OH)_4]^{12+}$ where tetrahedral and octahedral cages are present [39]. The NU-1000 is characterized by the formula $[Zr_6(\mu_3\text{-}O)_4(\mu_3\text{-}OH)_4(OH)_4(OH_2)_4]^{8+}$, where pyrene-based linkers (1,3,6,8-tetrakis(*p*-benzoic-acid)pyrene, H_4TBAPy) form characteristic triangular and hexagonal pores [39]. It should be also emphasised that the structure of UiO-66 may be rich in structural defects in the form of the missing linker or missing node which makes the overall structure far from "ideal" [40]. In this study for comparison reasons, the UiO-66 and UiO-$66_{25\%\ HCl}$ samples were synthesised, where increasing amounts of concentrated hydrochloric acid were used to increase structure defectivity.

In this paper, inspired by the achievements in the field of MOFs and their successful use as adsorbents for hazardous materials so far, we present a comprehensive study on the use of zirconium-based MOFs as an efficient adsorbent of 4-MMC which is a step forward to their application in detoxification in an acute drug overdose. Despite numerous literature reports on the use of MOFs, their composites, or derivatives, the information about their use for the adsorption of illicit drugs is scarce. The current literature describes the use of MOFs for the removal of mainly commonly used medicaments such as personal care products (PCP), analgetic, or antibiotics. The instant development of MOF syntheses and their application for medical purposes requires in-depth characterization by using living organisms.

More importantly, the effect of the use of MOFs as efficient 4-MMC adsorbents on living organisms has not been described in the literature before. Based on experimental and theoretical considerations we answer key questions: i) whether zirconium-based MOFs may be successfully used for the removal of 4-MMC from aqueous solution, ii) what are the mechanisms describing the adsorption of 4-MMC in prepared UiO-66 and NU-1000 MOFs, and finally iii) are the MOFs potentially safe for the use in living organisms in 4-MMC detoxification treatment?

Therefore, we present for the first time, according to our best knowledge, the usability of MOFs as sorbents of a wide range of drugs, and the use of the fish larvae as the detectors of the detoxification efficiency (removal of drugs of abuse), and, simultaneously, the low toxicity and cardioprotective effects of the studied MOFs.

2. Experimental

The materials used in this study were reagent grade and used without further purification. A detailed list of the reagent used in this study is provided in Supplementary Information File.

2.1. Material synthesis and characterization

The zirconium-based MOFs used in this study: UiO-66, UiO-$66_{25\%\ HCl}$, and NU-1000 were prepared according to the procedures described previously in the literature [18,37]. The synthesis protocols are provided in the Supporting Information File. The prepared MOF materials as well as the samples after sorption of 4-MMC, 4-MMC@MOF, were characterized by powder X-ray diffraction (PXRD), low-temperature nitrogen adsorption, dissolution ^1H nuclear magnetic resonance (NMR) spectroscopy, attenuated total reflectance Fourier transform infrared spectroscopy (ATR-FTIR), μRaman spectroscopy and scanning electron microscopy (SEM). Detailed characterization information is provided in the Supporting Information File.

2.2. Mephedrone adsorption studies

To determine the adsorption efficiency of 4-MMC on UiO-66, UiO-$66_{25\%\ HCl}$, and NU-1000, the kinetic studies were performed according to the procedure described in our previous work [18] with some modifications. The 4-MMC adsorption kinetic tests were performed by exposing 10 mg of previously activated MOF samples to 2 mL of 1000

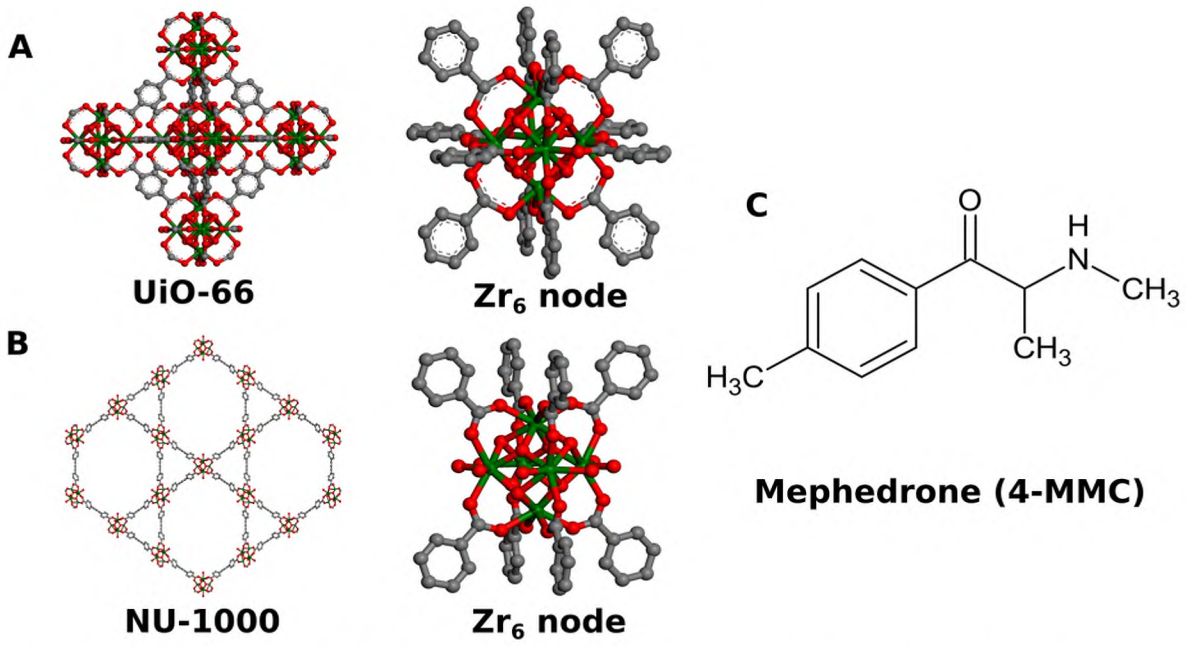

Fig. 1. Crystal structures and Zr_6 nodes in prepared Zr-based MOFs (**A**) UiO-66, (**B**) NU-1000, (**C**) mephedrone (4-MMC) structure.

μM 4-MMC aqueous solution under thermostatic conditions (25 °C). The 4-MMC concentrations were determined at specified time intervals by collecting the 0.1 mL solutions. The collected samples were diluted to the required concentration, centrifuged at 6000 rpm for 5 min, and measured by using a UV–Vis spectrometer (AvaSpec-ULS3648 high-resolution spectrometer). To determine the Freundlich adsorption isotherms, the experiments were performed by exposing 10 mg of previously activated MOF samples to 2 mL of 1000, 1500, and 2000 μM 4-MMC aqueous solution under thermostatic conditions (25 °C). The 4-MMC concentrations were measured as described above for 4-MMC kinetic experiments. The adsorption experiments were described by using pseudo-first and pseudo-second-order models using the equations previously described elsewhere [18,41]. The adsorption efficiency of 4-MMC on NU-1000 was also performed from 1000 μM 4-MMC from SBF solution under thermostatic conditions (25 °C). The SBF solution was performed according to the procedure described elsewhere [42]. The adsorption and 4-MMC concentration determination protocols were as described above.

To determine Q_{max}, the experiments were performed by exposing 10 mg of previously activated MOF samples to 2 mL of 250, 500, 750, 1000, 1500, and 2000 μM 4-MMC aqueous solution under thermostatic conditions (25 °C). The 4-MMC concentrations were measured as described above for 4-MMC kinetic experiments. To obtain Q_{max} values, the dual-site Langmuir model was applied [43].

To demonstrate the sequential purification of 4-MMC solution with MOF adsorbent, the cascade 4-MMC adsorption studies were performed for the most efficient adsorbent - NU-1000. In this experiment, the 10 mg of the previously activated MOF sample was added to 2000 μM 4-MMC aqueous solution for 24 h under thermostatic conditions (25 °C). After that time, the resulting 4-MMC concentration was measured spectrophotometrically. The 4-MMC solution after the adsorption process was centrifuged at 6000 rpm for 5 min to remove MOF with adsorbed 4-MMC and the fresh-activated 10 mg MOF sample was added to the 4-MMC solution. The procedure was triple repeated. Prior to the adsorption experiments, the MOF sample was activated in a vacuum oven at 120 °C for 12 h.

The additional recyclability experiments on purification of 4-MMC solution with 4-MMC adsorbent were performed for NU-1000 with the regeneration of spent NU-1000 in the previous regeneration step. In this experiment, the 10 mg of the previously activated MOF sample was added to 1000 μM 4-MMC aqueous solution for 24 h under thermostatic conditions (25 °C). After that time, NU-1000 was separated from the solution by centrifugation at 6000 rpm for 5 min. Subsequently, the spent NU-1000 sample was regenerated by soaking in methanol for 1 h under vigorous stirring. After that time, the NU-1000 was centrifuged, dried under ambient conditions overnight, and subsequently dried under vacuum at 120 °C for 10 h. The recycling procedure was triple repeated.

2.3. Periodic density functional theory (DFT) calculations

The adsorption process was modeled at the quantum-chemical Density Functional Theory (DFT) level with the periodic boundary conditions with the use of the VASP package [44,45]. The computational details concerning both the methodology and the models are given in the Supplementary Information file. The geometrical relationship between the planes of the aromatic ring of the 4-MMC molecules and the aromatic platform of the MOF hosts were described in the view of their π-π orbitals, and the interaction energetics was rationalized as the π-π orbital stacking (in the parallel or the staggered/parallel-displaced geometry). The geometric relationship has been determined by the analysis of the average (as the least squares fit) planes of the aromatic rings.

2.4. In vivo studies

2.4.1. Zebrafish maintenance

Danio rerio of the AB strain (Experimental Medicine Centre, Medical University of Lublin, Poland) was maintained as described previously [46]. For the experiments, the embryos were treated with 4-MMC (25 or 200 μM) alone and with MOFs in a sterile E3 medium at 28.5 °C, for 24 h. All experiments were conducted in accordance with the National Institute of Health Guidelines for the Care and Use of Laboratory Animals and the European Community Council Directive for the Care and Use of Laboratory Animals of September 22, 2010 (2010/63/EU). The concentrations of 4-MMC were chosen based on our preliminary studies.

2.4.2. Ecotoxicity

To determine the toxicity of 4-MMC, the fish embryo toxicity (FET) test was performed on *Danio rerio* according to OECD Test Guideline 236 [47]. Briefly, newly fertilized zebrafish eggs were exposed to 4-MMC alone or with MOFs for a period of 96 h at concentrations ranging up to 900 μM. The system applied in the experiment was static, as the changes in solution concentrations did not exceed the range of 20% of nominal concentration values. The following endpoints after 96 h incubation were noticed: the coagulation of fertilized eggs, lack of somite formation, lack of detachment of the tailbud from the yolk sac, and lack of heartbeat. Based on mortality the value of LC_{50} was calculated. For the evaluation of cardiotoxicity of 4-MMC, the heartbeat per minute (bpm) was measured.

2.4.3. Locomotor activity assay

The test was performed on 5 days post fertilization (dpf) larvae. Larvae were incubated in 4-MMC solution (200 μM), or 4-MMC (200 μM) + MOFs for 30 min. Then one larva per well was placed in 96 multi-well plates in E3 solution (each group of n = 20). After 5 min of habituation, EthoVision XT 15 video tracking software (Noldus Information Technology b. v., The Netherlands) was used for the evaluation of the locomotor activity. The distance moved in 10 min period was calculated in cm, in a light condition.

2.4.4. Color preference assay

The test was performed on 5 days post fertilization (dpf) larvae. The equipment consists of three types of Petri's plate: 1) with a blue-coloured bottom; 2) with a yellow-coloured bottom; 3) with a bottom divided into two equal parts blue and yellow. One larva per well was placed on a plate. Our preliminary studies showed that 5 dpf larvae prefer blue to yellow (Supporting Information). The test consists of phases.

1) Evaluation of initial preference (pre-test) – incubation on a plate with the bottom divided into two equal parts – blue and yellow (5 min)
2) Conditioning:
   a. incubation in a more preferred (blue) coloured plate with E3 solution (5 min);
   b. incubation in less preferred (yellow) in 4-MMC solution (25 μM), MOFs solution, or 4-MMC (25 μM) + MOFs (5 min);
3) Evaluation of final preference (test) - incubation in a plate with the bottom divided into two equal parts blue and yellow (5 min).

Time spent on yellow and blue parts was evaluated in the first and third steps of the experiment during a 5 min period using EthoVision XT 15 video tracking software, in a light condition.

For statistical analysis, Prism software (GraphPad Software, San Diego, CA) was used. Data were presented as mean ± SEM. Data were analyzed using a two-way analysis of variance (ANOVA). For the color preference test, a SCORE was calculated, *i.e.*, the differences between post-conditioning and pre-conditioning time spent in the drug-associated (yellow) part of the plate.

3. Results and discussion

3.1. Synthesis and characterization

The successful preparation of Zr-based MOF materials was confirmed with PXRD analysis (Fig. 2A). The comparison of PXRD patterns of prepared MOF materials with the literature data confirms their high crystallinity [48,49].

The porous structure of prepared materials was confirmed by low-temperature N_2 adsorption experiments (Fig. 2 B, C). According to the IUPAC classification the nitrogen adsorption isotherms of UiO-66 and UiO-$66_{25\%\ HCl}$ were I-type and the biggest increase in sorption capacity was obtained in the range $0 < \frac{p}{p^0} < 0.05$. For NU-1000 IV-type isotherm was observed and the ranges of greatest increase in sorption capacity were in a range of $0 < \frac{p}{p^0} < 0.05$ and $0.25 < \frac{p}{p^0} < 0.3$. Additional hysteresis of H2-type was also noticed. Based on the N_2 adsorption equilibrium points, the structural parameters were calculated (Table 2). The specific surface area S_{BET} and S_{Lang} were determined based on the multilayer and single-layer filling model, respectively [50,51]. For UiO-66, the specific surface area S_{BET} was 1060 m^2/g and S_{Lang} was 1517 m^2/g. The use of the higher amount of hydrochloric acid as a modulator for the synthesis of UiO-$66_{25\%\ HCl}$ resulted in structural changes and an increase in surface area values to S_{BET} = 1278 m^2/g and S_{Lang} = 1803 m^2/g, respectively. The total volume of meso- and fine macropores were 0.08 cm^3/g for UiO-66 and 0.32 cm^3/g for UiO-$66_{25\%\ HCl}$ samples with average pore diameters of 4.9 nm and 14.5 nm, respectively. In the case of NU-1000, the determined S_{BET} was equal to 2259 m^2/g whereas S_{Lang} was 4095 m^2/g, which is in agreement with the literature data [52]. The pore volume V_{BJH} was much higher than that of UiO-$66_{25\%\ HCl}$ and reached 1.07 cm^3/g and the D_{BJH} = 2.5 nm. The pore size distribution (PSD) for MOFs was carried out based on the NLDFT model (Fig. 2C). The NU-1000 exhibited increased pore volume with diameters in the range of 2.1–3.0 nm and one dominant peak in the pore size of 3.2–3.8 nm with increased volume. These pore sizes correspond to mesopores in the lower diameter size range, and NU-1000 can be considered a mesoporous material. The volume of micro- and mesopores was 1.26 cm^3/g. A peak of increased pore volume in the range 0.5–1 nm was detected for UiO-66 and two peaks in the ranges: 0.8–1.2 nm and 1.5–2.0 nm in the UiO-$66_{25\%\ HCl}$ sample.

The molecular nature of prepared MOFs samples before and after the 4-MMC adsorption from aqueous 4-MMC solution was determined by transmission FTIR and μRaman spectroscopies. The results of the FTIR analysis of crystalline 4-MMC and MOF samples after 4-MMC adsorption are shown in Fig. 3A. The broadband in a range of 3000–2500 cm^{-1} may be attributed to ring stretching vibrations. The band at 2715 cm^{-1} can be attributed to NH_2 vibrations [53]. The most characteristic band at 1689 cm^{-1} originates from stretching vibrations of the carbonyl group [53]. The FTIR spectra of pristine MOF samples showed typical vibrations for UiO-66 and NU-1000 that can be found in the literature. The obtained results support the diffraction patterns obtained by PXRD analyses. The broad band at 3500-2500 cm^{-1} may be attributed to OH vibrations of adsorbed water. The small bands in a 3000 cm^{-1} region originate from CH modes from benzene rings [54]. The most characteristic bands at 1585 and 1395 cm^{-1} correspond with in- and out-of-phase stretching vibrations of carboxylate groups. The bands in the 750-650 cm^{-1} range originate from OH and CH bending and Zr–O modes [54]. The transmission FTIR spectra of MOF samples after 4-MMC show band broadening in a 4-MMC fingerprint region which is an effect of overlapping of both metal-organic frameworks and adsorbed 4-MMC molecules. The predominant band broadening was observed for the 4-MMC@NU-1000 sample, for which the highest 4-MMC loading was determined. More importantly, the marking band at 1689 cm^{-1} originating from 4-MMC C=O vibrations considerably increases in the case of the 4-MMC@NU-1000 sample (Fig. 3A) which indicates successful 4-MMC adsorption. The analysis of μRaman spectra of pure and MOF samples after 4-MMC adsorption are shown in Fig. S1 A and Fig. S1 B. The μRaman spectra of both NU-1000 and UiO-66 are in good agreement with the literature data [55,56]. Parent NU-1000 sample shows bands at 1180, 1160, 900, 840, and 430 cm^{-1} which correspond with pyrene-based ligand vibrations [55]. While UiO-66 exhibited characteristic bands at 1621, 1454, 1434, and 1135 cm^{-1} which are attributed to C–C aromatic stretching, O–C–O carboxylate stretching, C–C stretching from carboxylate and C–C symmetric breathing, respectively. The Raman spectrum of pure 4-MMC (Fig. S1 B) shows bands at 1678, 1606, 1184, and 804 cm^{-1} which correspond with C=O stretching, C=C stretching, asymmetric C–N–C stretching, and benzene ring vibrations, respectively [57]. The μRaman spectra of MOF samples after 4-MMC adsorption do not show the signals from 4-MMC probably due to the overlapping of characteristic bands of both MOFs and 4-MMC or

Table 2
Sample characteristics.

Parameter		Unit	UiO-66	UiO-$66_{25\%\ HCl}$	NU-1000
Sorption capacity at 0.1 MPa	a	cm^3/g STP	336.0	603.3	835.8
BET surface area	S_{BET}	m^2/g	1060.0 ± 22.9	1278.0 ± 42.2	2258.5 ± 188.6
Langmuir surface area	S_{Lang}	m^2/g	1516.5 ± 1.7	1802.6 ± 2.4	4095.2 ± 131.7
BJH surface area	S_{BJH}	m^2/g	63.5	88.3	1703.6
BJH total pore volume[a]	V_{BJH}	cm^3/g	0.08	0.32	1.07
BJH adsorption average pore width	D_{BJH}	nm	4.9	14.5	2.5
NLDFT total pore volume[b]	V_{NLDFT}	cm^3/g	0.55	0.66	1.26
Maximum 4-MMC loading[c]		wt%	24.01 ± 0.37	35.17 ± 1.74	44.75 ± 3.22

where.
[a] pores with a width of 1.7 nm–300 nm.
[b] pores with a width of less than 23.7 nm.
[c] in a single adsorption experiment 10 mg MOF/2 mL 1000 μM 4-MMC aq. Solution at 25 °C.

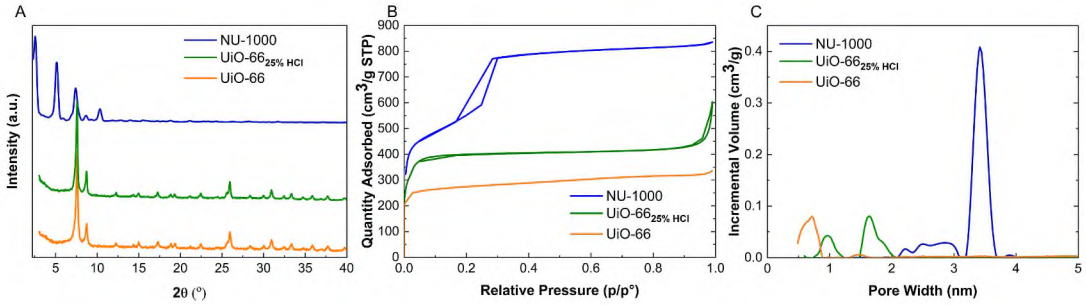

Fig. 2. (A) PXRD; (B) N_2 adsorption isotherms; (C) DFT pore size distribution.

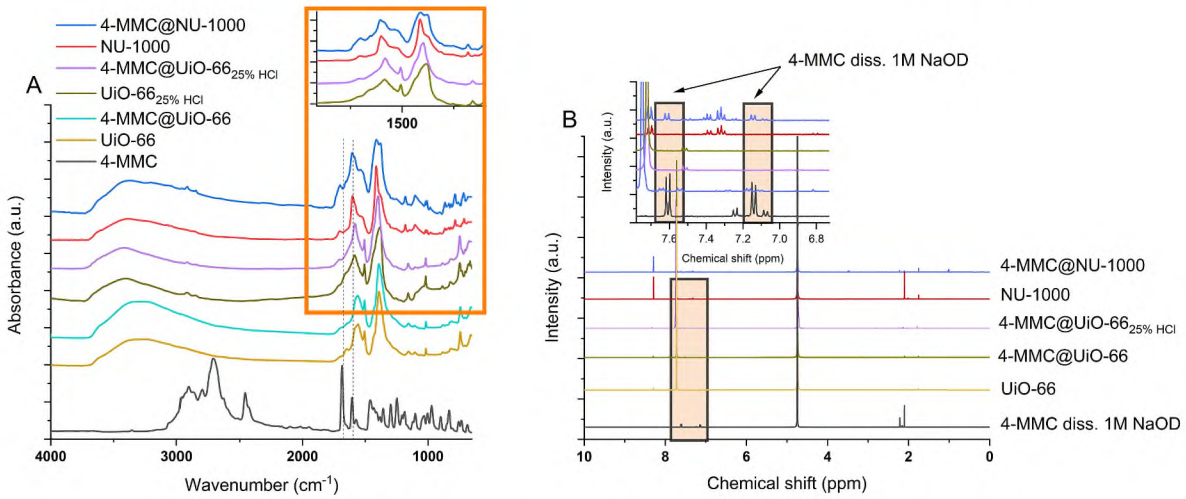

Fig. 3. (**A**) Transmission FTIR spectra of 4-MMC@MOF samples; (**B**) ^{1}H NMR spectroscopy results.

because there is not enough 4-MMC adsorbed to give a good Raman signal in MOF matrix. In work by Mabott et al. [57] the analysis of 4-MMC performed by Surface-Enhanced Raman Scattering shows its great advantage in the determination of 4-MMC even at concentrations as low as 1.6 μg/mL. Although the concentrations of 4-MMC in our samples exceeds LOD determined by Mabott et al. [57], in our study we performed conventional μRaman analysis and the work of Mabott et al. [57] does not consider the complex MOFs matrix.

The complexity of our system pushed us to design the spectroscopic measurement which will allow us to detect the 4-MMC in the MOF matrix. Based on previous work by Shearer et al. [49] we applied dissolution ^{1}H NMR spectroscopy, to digest the MOF matric to determine the presence of 4-MMC adsorbed in MOF pores. The results of dissolution spectroscopy are presented in Fig. 3B and Figs. S2–S6. The ^{1}H NMR spectrum of 4-MMC diluted in 1 M NaOD (Fig. 3B, Figure exhibits signals at δ 7.61 (d, $J = 8.2$ Hz, 1H), 7.14 (d, $J = 7.9$ Hz, 1H), 2.22 (s, 3H), 2.11 (s, 3H) and correspond with the ^{1}H NMR spectrum of 1-(4-methylphenyl)-1,2-propanedione (MPPD) which is degradation the product of 4-MMC at highly basic conditions which were applied during the MOF digestion [58,59]. The degradation pathways of 4-MMC under basic conditions were recently described in work by Tsujikawa et al. [58]. In their work, the degradation mechanism of 4-MMC in the pH = 12 buffer after 0, 6, 12, and 48 h of storage was determined by using the GC-MS method. They found that under those conditions 4-MMC degrades to the following molecules in order: 4-MMC - > MPPD - > MBA - > DMBA (MPPD: 1-(4-methylphenyl)-1,2-propanedione; MBA: 4-methylbenzoic acid; DMBA: N, 4-dimethylbenzamide), respectively. To confirm the purity of pristine 4-MMC and its decomposition under highly basic conditions that were used for our study, we performed the ^{1}H NMR. The experimental ^{1}H NMR and ^{13}C NMR spectra of 4-MMC are in good agreement with the literature [53,58,60] data and simulated patterns (Figs. S2–S6). One could expect that under these conditions after 12 h of digestion, the ^{1}H NMR gives the signals for DMBA rather than MPDD as suggested by Tsujikawa et al. [58]. It must be kept in mind, however, that 4-MMC was adsorbed in the MOF matrix and the exact time of interaction of NaOD was shorter than 12 h due to its reaction with MOF's framework.

The electronic structure of pristine and MOFs after 4-MMC adsorption was determined by DR UV–Vis spectroscopy (Figs. S7–S8). Upon adsorption of 4-MMC, the bathochromic effect (for NU-1000) or hypsochromic (for UiO-66) effects were observed, and its interpretation as the result of the π-π orbital interaction is analogous to that recently noted by Sun et al. [61] in the porous pyrene-based organic cage where the C–H … π interaction took place.

The morphology of the MOF samples after the 4-MMC adsorption is shown in Fig. 4. The MOF samples showed morphology that was previously reported in the literature for NU-1000 and UiO-66 samples [36,52]. The NU-1000 may be characterized as 3 μm (diameter) crystals in a form of a hexagonal prism. The UiO-66$_{25\%\ HCl}$ and UiO-66 samples were detected as agglomerated crystals with ca. 2 μm size. It must be emphasised that the morphology of MOFs is strongly affected by the synthesis parameters. As previously described in the literature [49,62] the size and the morphology of the resulting MOF can be tuned by the choice of the modulator concentration and acidity. As shown by Shearer et al. [49], the morphology of crystals of UiO-66 becomes more distinct and the crystals in the form of the octahedron are mostly detected with increasing molar equivalents of the organic modulator used during the synthesis. When analysing the SEM images of UiO-66$_{25\%\ HCl}$ and UiO-66 after the 4-MMC adsorption (Fig. 4 B, C) we did not observe the changes in the morphology of MOFs in comparison with their pristine counterparts.

The adsorption properties of 4-MMC were tested on UiO-66, UiO-66$_{25\%\ HCl}$, and NU-1000 samples (Fig. 5 A). The most efficient adsorption of 4-MMC takes place in the first 1 h of adsorption. In the first 5 min of 4-MMC adsorption from 1000 μM solution, the adsorption was equal to 8.7, 5.1, and 3.0 mg/g for NU-1000, UiO-66$_{25\%\ HCl}$, and UiO-66, respectively. It must be emphasised, that the beneficial effect of the modulated synthesis on the adsorption efficiency in the case of UiO-66 family samples may be observed in the first 1 h of the adsorption process. In the case of UiO-66$_{25\%\ HCl}$ modulated synthesis with hydrochloric acid causes easier access to the MOF channels, which is reflected in the greater sorption capacity for 4-MMC molecules. This phenomenon may be also observed with the overall adsorption efficiency of UiO-66$_{25\%\ HCl}$ giving the final 4-MMC loading equal to 24.01 ± 0.37 wt%. On the other hand, when considering the prepared materials in terms of their potential application for the removal of 4-MMC during their overdose, the adsorption profile should have a much gentler growth and high overall adsorption spread over time. Such requirement is met by NU-1000 which at 1 and 2 h of adsorption efficiency places in between UiO-66 and UiO-66$_{25\%\ HCl}$, whereas its maximum loading is twice as high as for UiO-66 reaching 22.9 mg/g. The detailed kinetic parameters of the 4-MMC adsorption are also shown for UiO-66$_{25\%\ HCl}$ and NU-1000 samples in the form of detailed calculated pseudo-first order and pseudo-second order kinetic curves fitted to Freundlich adsorption model (Figs. S9–S11, Table S1).

To determine the 4-MMC adsorption process in living organisms, the adsorption experiments for the most efficient sample - NU-1000 were also performed in the simulated body fluid solution (SBF) (Fig. 5A). It may be found that the overall adsorption efficiency is almost 1.5 times higher than in the case of the adsorption of 4-MMC from water solution.

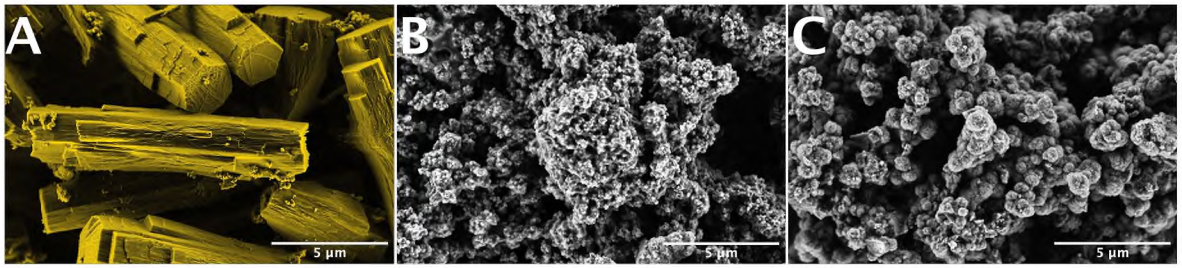

Fig. 4. SEM images of prepared samples after 4-MMC adsorption; × 25 k magnification; **(A)** 4-MMC@NU-1000; **(B)** 4-MMC@UiO-66$_{25\%\ HCl}$; **(C)** 4-MMC@UiO-66

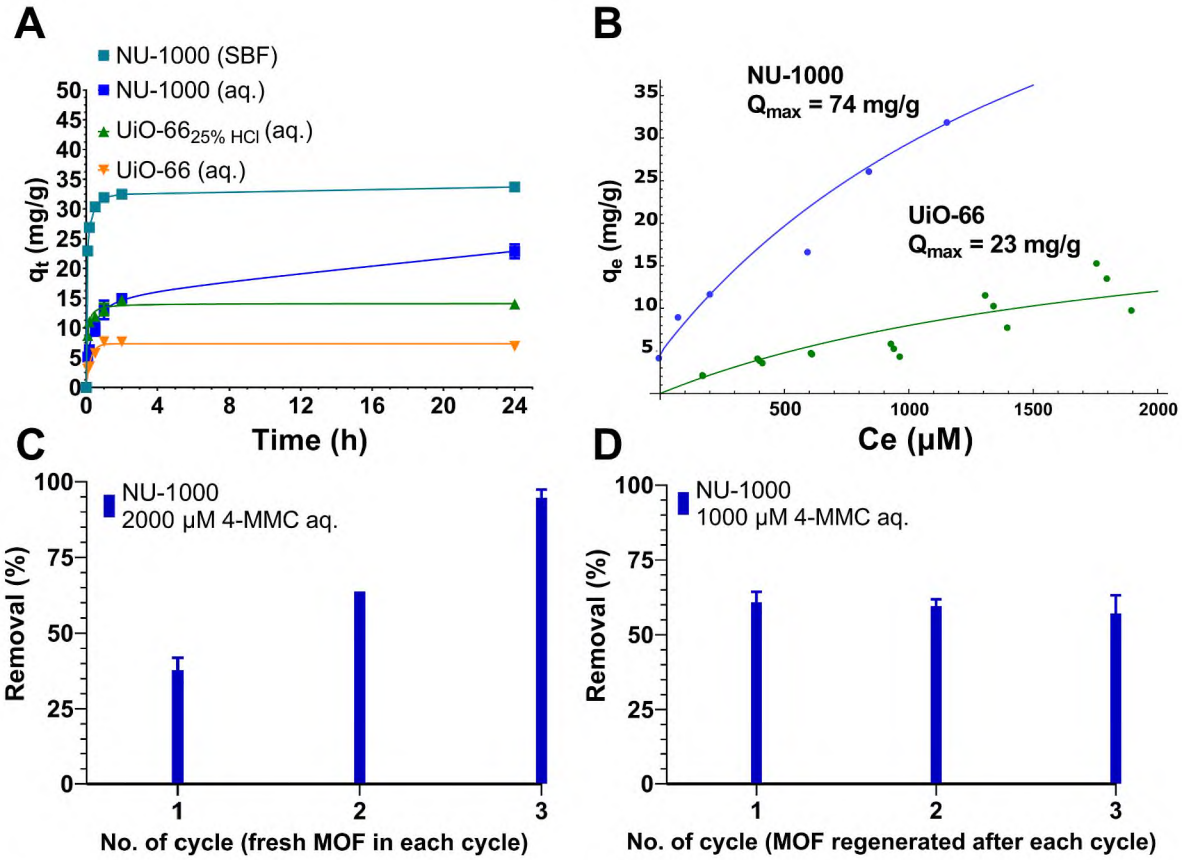

Fig. 5. **(A)** 4-MMC removal efficiency on prepared Zr-MOFs, **(B)** equilibrium loading in prepared Zr-MOFs, **(C)** 4-MMC cascade removal efficiency on NU-1000 sample from 2000 μM solution (fresh MOF was used in each cycle), **(D)** 4-MMC cascade removal efficiency on NU-1000 sample from 1000 μM solution (MOF was regenerated after each cycle and reused).

Following the findings in the literature [63], it can be presumed that in our case the analogous functionalisation of NU-1000 by the SBF solution may lead to the formation of hydroxyapatite (HA) on the MOF surface. The differences in surface charge distribution, imposed by the presence of various ions in SBF solution, favour the 4-MMC adsorption. As evidenced in the work of Höhn et al. [63], the soaking of bioglasses in SBF solution turns the inert structure into the biocompatible, charged surface with enhanced human serum albumin (BSA) adsorbents. In other work by Liu et al. [64], the SBF surface functionalisation was performed to obtain a carbonated hydroxyapatite layer to improve the bioactivity of bio-MOF-1.

To further test the hypothesis whether the ions that form the SBF solution were also adsorbed together with the 4-MMC molecules from the SBF solution, the EDS elemental analysis of pristine NU-1000 and NU-1000 after 4-MMC adsorption form SBF solution was performed (Table 3). As it can be inferred, the elements that are present in an ionic form in an SBF solution (Na, K, Ca) were not detected in the pristine NU-1000 sample. In contrary, in NU-1000 sample after 4-MMC adsorption the elements like Na, K or Ca were detected. Moreover, the prominent element that is present in the SBF solution – Na, was detected as 3.74 wt %. Indeed, it is worth mentioning that the values obtained from the EDS analysis should be treated as semi-quantitative rather than qualitative. However, the presence of the surface charge induced by SBF can be a rationale for the enhanced sorption properties in SBF, as previously

Table 3
EDS analysis results for parent NU-1000 and NU-1000 after 4-MMC adsorption from SBF solution.

Pristine NU-1000 (NU-1000 after 4-MMC adsorption from SBF solution)		
Element	Atomic %	Weight %
Na	0.00 (2.18)	0.00 (3.74)
K	0.10 (0.31)	0.10 (0.52)
Ca	0.00 (0.21)	0.00 (0.52)

reported by Höhn et al. [63]. The obtained results give new insights into the research on 4-MMC adsorption and will be the subject of further research using other methods of MOF surface characterization. Another important factor that influences the 4-MMC adsorption is the structural defectivity of MOFs. According to the literature data, the structural defects may be engineered via several methods including modulated synthesis, temperature, Zr/ligand ratio, thermal activation, or metal cation substitution [65]. Numerous works have been devoted to defect generation through modulated synthesis, where numerous acids like benzoic acid, hydrochloric acid, acetic acid, or trifluoracetic acids are used [49,62,66–68]. According to the literature describing the structural defects in various MOFs, it may be observed that the determination of structural defects is challenging and require the application of numerous methods for the proper characterization of structure defectivity. In an exemplary work of Koschnick et al. [69] to describe the structure defects in Zr-based PCN-221 MOF, numerous methods were used including single-crystal X-ray diffraction (SCXRD), total scattering pair distribution function (PDF), Rietveld, and chemical analysis as well as solid-state nuclear magnetic resonance spectroscopy (ssNMR). In their work, they reveal that the $Zr_6O_4(OH)_4$ clusters in prepared PCN-221 may be misinterpreted as Zr_8O_6 clusters. Additionally, they found that in highly defective MOFs (up to 50% of linker vacancies), vacancy ordering may occur. Indeed, although in our work the considerable 4-MMC adsorption efficiency in UiO-6625% HCl and UiO-66 samples may be due to the generated structure defectivity in the modulated synthesis, the unambiguous determination of the number and nature of the generated structure defects would require the use of advanced characterization techniques as presented by Koschnick et al. [69].

To calculate the maximum loadings of 4-MMC in prepared NU-1000 and $UiO\text{-}66_{25\%\ HCl}$ samples (Q_{max}), the isotherms were calculated (Fig. 5B). As can be seen, the adsorption resembles the dual-site Langmuir model [43]. The calculated Q_{max} values were equal to 74 and 23 mg/g, for NU-1000 and UiO-66, respectively.

To determine the removal efficiency of 4-MMC we performed the 3-cycle experiment consisting of three-fold purification of the starting 2000 μM 4-MMC aqueous solution (Fig. 5C). Such an approach is dictated by the potential application of Zr-MOFs for 4-MMC controlled, gradual withdrawal (detoxification) from living organisms. For that reason, although a cyclic administration of the adsorbent may increase the costs of the entire treatment, it is commonly practiced in the case of adsorption of intoxicants by, e.g., active carbon [70]. Following this way of thought, to simulate the multiple dosing of the adsorbent during a clean-up treatment, 3-step adsorptive removal of 4-MMC with fresh MOF is proposed. In each step after 24 h of adsorption, the spent NU-1000 was replaced by a fresh MOF sample, and the adsorption was continued for the next 24 h. The results of the 4-MMC removal by triple dosing of 4-MMC clearly show that the 4-MMC is successfully removed from the aqueous solution. The gradual removal of 4-MMC in the presented way allows to avoid withdrawal effects such as increased anxiety, depression, digestive problems, or tremors, which can occur in highly addicted people [71]. The additional experiment showing the possible application of NU-1000 to the adsorptive removal of 4-MMC from aqueous solution was performed, where the NU-1000 sample was regenerated after each adsorption cycle and regenerated MOF was reused for the adsorptive removal of 4-MMC (Fig. 5D). As shown in Fig. 5D, the adsorption efficiency remains at the same level reaching ca. 60% in each recycle cycle.

3.2. *Mephedrone loading – a DFT computational approach*

To comprehensively understand the mechanisms of the adsorption of 4-MMC over prepared samples we performed DFT calculation. The optimized models of 4-MMC adsorbed on prepared material are shown in Fig. 6 and Figs. S12–S16. The calculated sorption energies are shown

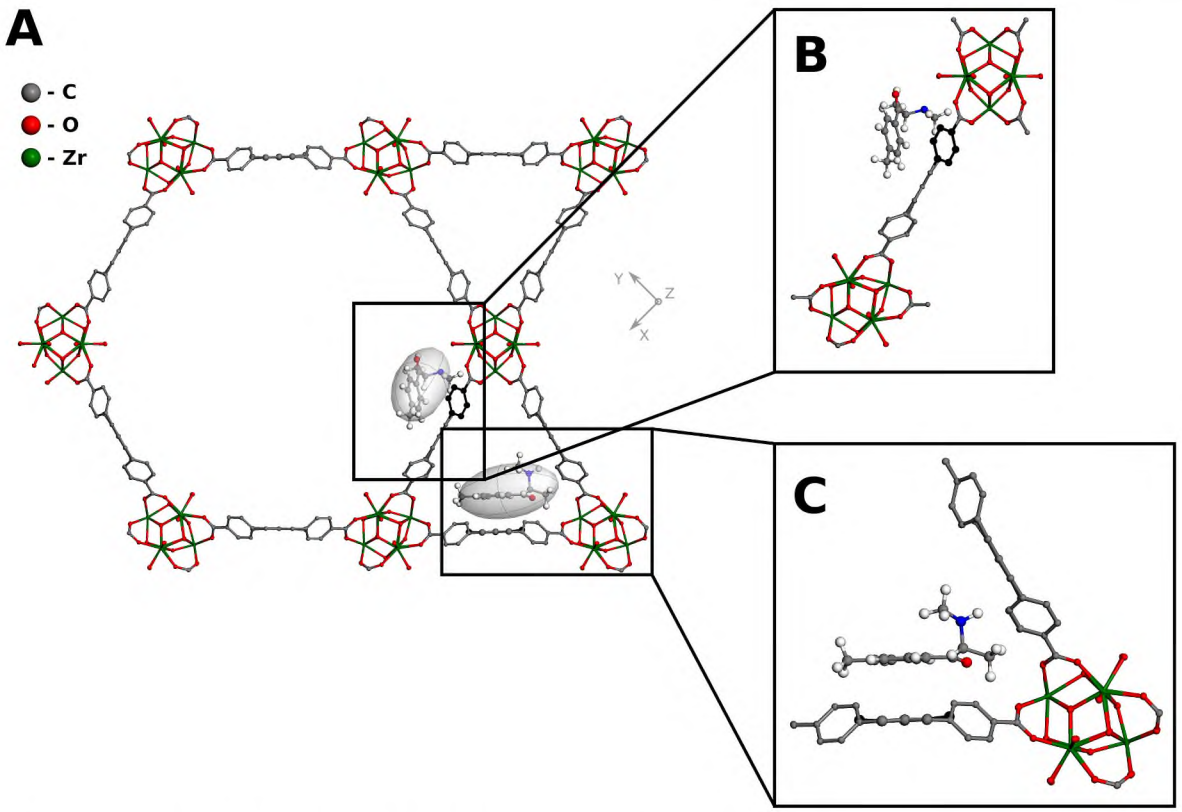

Fig. 6. DFT optimized structure of NU-1000, in zoomed region the adsorbed 4-MMC molecules are marked as ellipsoids; **(A)** general model, **(B)** zoomed large channel with adsorbed 4-MMC, **(C)** zoomed small channel with adsorbed 4-MMC; hydrogens omitted for clarity; green – Zr, red – O, grey – C, blue – N; additional DFT optimized structures are provided in the Supplementary Information File.

in Table S2.

The equilibrium loading was estimated by means of the Monte-Carlo (MC) simulations in the temperature of 298 K, with the use of the Metropolis algorithm and with Universal Force Field (UFF) (Table S3). The isotherms were modeled for fugacity up to 100 kPa. The rigid host approximation was used, and it can rationalize the underestimation of the modeled loading for the MOF structures with tight channels.

Besides the sorption isotherm, the MC/UFF simulations were also used for the crude determination of the optimal sorption sites of the MOF structures. Such qualitative pre-screening was unavoidable due to the size of the phase space (positions and orientation of the sorbent molecule) that should be sampled. The obtained positions of 4-MMC molecules in MOF matrices were subsequently refined at the DFT+D level of theory with the use of the VASP code [44,45] (see SI for details). Such an approach was deemed appropriate as was shown in our previous article [36].

The geometrical relationship between the aromatic ring of the 4-MMC molecules and the aromatic rings of the MOF linkers was described in view of their π-π orbital stacking (see Table S4 and Fig. S16). The geometric descriptors have been determined by the relative position of the average (as the least squares fit) planes of the aromatic rings.

Based on the Monte Carlo force-field simulations, 3 stable locations of 4-MMC molecule in the large channel of NU-1000 and 1 stable position in the small channel have been found and further reoptimized at the DFT+D level of theory. Out of the 3 former locations, the most stable one is characterized by the strongest adsorption, $E_{ads} = -0.897$ eV, while for the latter position, the sorption is slightly weaker, $E_{ads} = -0.882$ eV. In the case of 4-MMC sorption in UiO-66, the adsorption was stronger and the optimal position of the adsorbate gave $E_{ads} = -2.528$ eV.

For the sake of comparison, the other drugs (fentanyl, cocaine, and morphine) have been used in the sorption modeling and hence the representability of 4-MMC sorption in NU-1000 and UiO-66 has been shown (Table S3). Namely, the Monte-Carlo rigid host modeling has been performed and the resultant positions of drug molecules in the MOF frameworks have been refined by the DFT optimization. Upon comparing the modeled sorption to the experimental data, it can be clearly seen that the studied MOFs can be used as generic sorbents of a wide set of abused drugs.

3.3. Metal-organic frameworks display protection against 4-MMC toxicity and cardioprotective properties

The use of MOFs allowed for avoiding developmental malformation at 1000 μM mephedrone and saved from death at higher mephedrone concentrations (Fig. 7A and B, Fig. S17). Based on our study we observed the protective effects of MOFs on 4-MMC treatment (Fig. 7 B). Out-of-toxicity tests revealed the dose-dependent influence of 4-MMC on the development of heart malformations and dysfunctions (Fig. 8 A, B). With increasing 4-MMC doses, we have observed the occurrence of heart malformation starting at 300 μM and disturbances in heart functions (heart rate) even earlier, at 150 μM. Moreover, the use of MOFs significantly improved heart functions, measured as heart rate, after 4-MMC administration at doses 200 and 250 μM (Fig. 8C and D).

3.4. The effect of metal-organic frameworks on the expression of mephedrone-induced locomotor activity and color preference

Locomotor activity tests revealed that MOFs, statistically significant, influence on locomotor activity of 5 dpf zebrafish [two-way ANOVA: MOF pretreatment F (3, 149) = 5.952; p = 0.0023, 4-MMC treatment F (1, 149) = 13.60; p = 0.0014, MOF treatment × 4-MMC treatment F (3, 149) = 13.45; P < 0.0001, Fig. 9 A, Fig. S18]. Post hoc Tukey's showed that 4-MMC (200 μM) increased observed parameter ($p < 0.001$) in comparison with E3 treated control group, whereas 4-MMC molecules in MOFs: UiO-$66_{25\%\ HCl}$ ($p < 0.001$), UiO-66 ($p < 0.001$), and NU-1000 ($p < 0.05$) decreased hyperlocomotion in 5 dpf zebrafish as compared with 4-MMC treated group. None of the used MOFs change locomotor activity as compared with E3 treated control group.

Fig. 9B indicates the effect of MOFs on the expression of 4-MMC-induced color preference in 5 dpf zebrafish [two-way ANOVA: MOF pretreatment: F (3, 139) = 6.042; p = 0.0009; 4-MMC - treatment: F(1, 139) = 0.4934; p = 0.4845; interaction: MOF treatment × 4-MMC - treatment: F(3, 139) = 5.968; p = 0.0010]. As the results showed, incubation in 4-MMC (25 μM) in the initially non-preferred part of the plate (yellow) increased the time spent in this part during the test time ($p < 0.05$). The addition of 1 mg of MOF to the 4-MMC solution reverse this color preference during the test day: UiO-$66_{25\%\ HCl}$ ($p < 0.05$), UiO-66 ($p < 0.05$), and NU-1000 ($p < 0.05$). None of the used MOFs changed color preference as compared with E3 treated control group. In vivo studies show, for the first time, that MOF matrices prevent toxic, cardiac as well as central nervous system effects of 4-MMC.

4. Conclusions

In this work, we aimed at the application of metal-organic frameworks for the efficient removal of novel psychoactive substances-mephedrone. The successful 4-MMC adsorption was performed on UiO-66, UiO-$66_{25\%\ HCl}$ prepared under modulated synthesis with hydrochloric acid and NU-1000 MOFs. The adsorption tests revealed that the adsorption kinetics is not only a derivative of MOF pore volume but is correlated with the structure of the MOF and 4-MMC location in MOF pores. Among prepared MOFs, NU-1000 achieved maximum 4-MMC adsorption, reaching 44.75 wt%. More importantly, the NU-1000

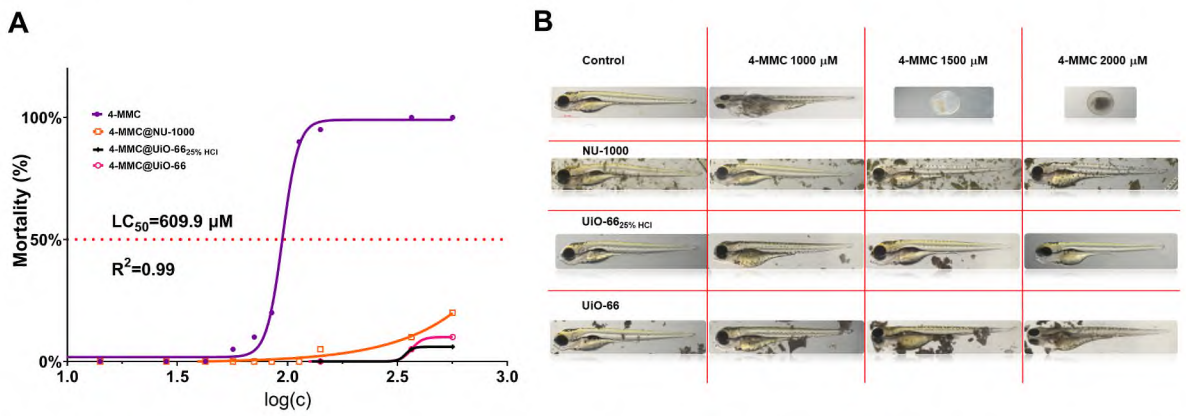

Fig. 7. Toxicity of 4-MMC alone and with MOFs. **(A)** the value of LC50 for 4-MMC at 96 hpf. **(B)** Effectiveness of MOFs: NU-1000, UiO-$66_{25\%\ HCl}$, UiO-66, against toxicity of 4-MMC at 1000, 1500 and 2000 μM.

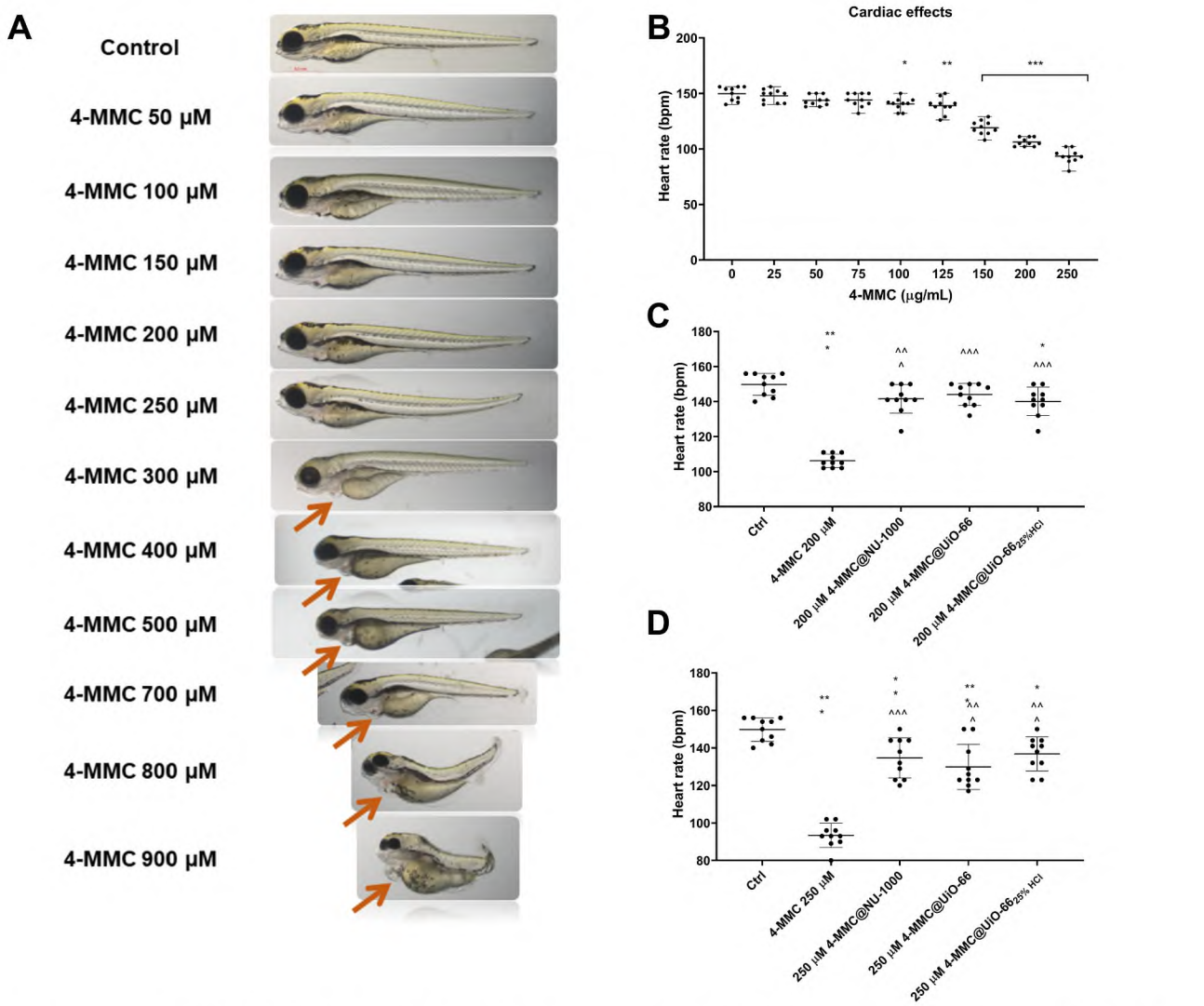

Fig. 8. Cardiotoxicity of 4-MMC in zebrafish. **(A)** Dose-dependent occurrence of heart developmental malformations – pericardial edema. **(B)** Cardiotoxic effects of 4-MMC expressed as heart beats per minutes (bpm). **(C)** Cardioprotective effects of MOFs: NU-1000, UiO-$66_{25\%\ HCl}$, UiO-66, against toxicity of 4-MMC at 200 μM, **(D)** Cardioprotective effects of MOFs: NU-1000, UiO-$66_{25\%\ HCl}$, UiO-66, against toxicity of 4-MMC at 250 μM. Data are presented as single values, mean ± SD. n = 20; *p *< 0.05; **p < 0.005, ***p < 0.001 vs E3 treated control group,* ∆p *< 0.05;* ∆∆p*<0.005;* ∆∆∆p*<0.001 vs* 4-MMC *treated group, post hoc Tukey's test.*

exhibited a mild adsorption profile, which is necessary when considering its potential application for the cathinone overdose treatment.

We found that the spectroscopic characterization of 4-MMC over Zr-based MOFs may be challenging due to molecular similarities between adsorbed 4-MMC and the molecules building MOFs structure. The overlapping of both metal-organic-frameworks and adsorbed 4-MMC molecules may blur the overall spectroscopic characterization of obtained systems and a comprehensive approach utilising several methods including FTIR, μRaman, ^{1}H NMR, DR-UV-Vis and DFT studies provide the actual state of the 4-MMC@MOFs system. Due to the both 4-MMC and MOFs overlapping, the characterization by conventional FTIR and μRaman techniques did not give unequivocal information about the system. The use of combined DR UV–Vis/^{1}H NMR allowed us to comprehensively characterize described systems.

The ^{1}H NMR dissolution spectroscopy results have confirmed that the 4-MMC was successfully adsorbed in prepared MOFs. The in-depth analysis of ^{1}H NMR has confirmed that under highly basic dissolution conditions, 4-MMC degrades to 1-(4-methylphenyl)-1,2-propanedione.

The DFT calculations showed that the 4-MMC can be adsorbed in the large channels of NU-1000 and the sorption energies were in the range of −0.345 eV to −0.775 eV in large channels whereas in the small channel, the sorption was stronger, and the energy was equal to −0.921 eV. The total bond order between the 4-MMC molecule and the MOF linker was in the range of 0.677–1.033 (large channel) and equal to 0.885 for the small channel. The charge transfer between the molecule and the linker was negligible (<0.08 atomic unit, to the absolute value) in all studied cases. The introduction of the polarizable continuum environment weakened the sorption in all cases, as expected.

The sorption in UiO-66 in its tight channel is much stronger, compared to NU-1000. The sorption energy is a few times higher (to the absolute value), which is caused by a much stronger perturbation of the electronic structure: the bond order between the 4-MMC molecule and the MOF linker is almost 1.5 and the charge transfer is significant, higher than 0.5 at. u. (partial electron density depletion of the 4-MMC molecule).

The *in vitro* and *in vivo* experiments have confirmed the low cytotoxicity of prepared MOFs. The superior cardioprotective and embryo protective effect of metal-organic frameworks has been confirmed by the *in vivo* experiments using the *Danio rerio* model organism. Based on experimental results the calculated LC_{50} of 4-MMC was equal to 609.9 μM. Furthermore, based on *in vivo* experiments we confirmed the cardioprotective effect of metal-organic frameworks which avoid cardiac

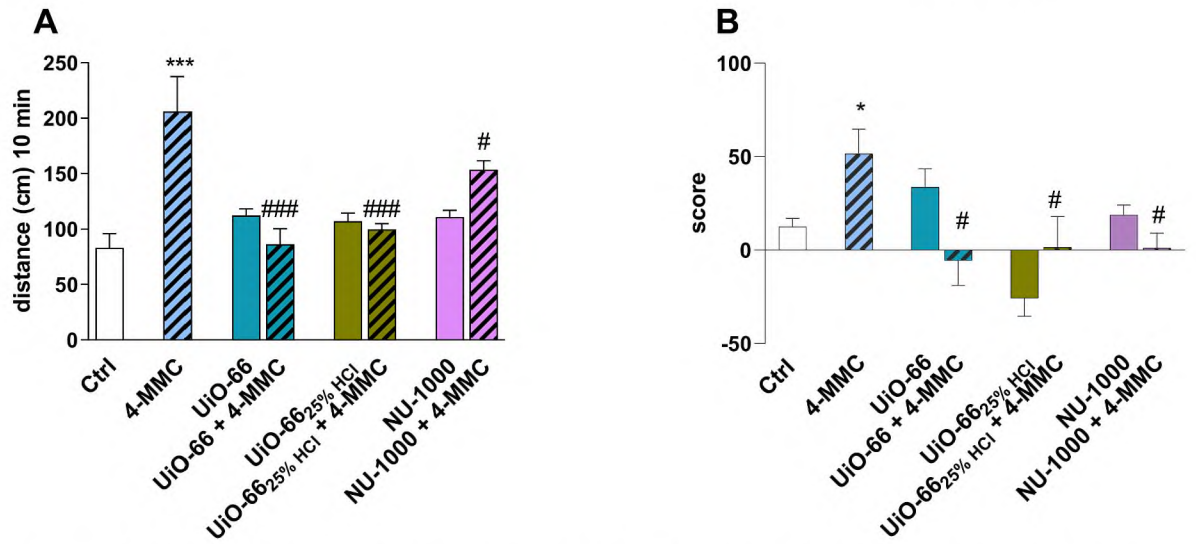

Fig. 9. (A) The effects of mephedrone (4-MMC, 200 μM), MOFs and 4-MMC + MOFs on distance moved by 5 dpf zebrafish larvae (in cm) under continuous illumination, **(B)** The effects of 4-MMC (25 μM), MOFs and 4-MMC + MOFs on zebrafish larvae color preference. Data are presented as mean ± SEM. n = 20; *p < *0.05;* ***p < *0.001 vs E3 treated control group,* #p < *0.05;* ###p<*0.001 vs* 4-MMC *treated group, post hoc Bonferroni's test.*

hypertrophy and the decrease of average heart rate at the concentration above 200 μM of 4-MMC.

Zebrafish larvae display swimming at 4–5 dpf, after the development of a swim bladder, and they exhibit a wide repertoire of behaviors such as memory, depression, aggression, anxiety, and social interaction [72–75]. Furthermore, neurons using serotonin, dopamine, and noradrenalin as neurotransmitters have been identified in the zebrafish central nervous system. Their eyes have cells in the retina similar to these of other vertebrates, including humans, and detect light from 3.5 dpf [76]. This small organism distinguishes a rich palette of colors, which is a clear advantage over rodents in behavioral studies [77]. The innate color preference of zebrafish was used to assess the rewarding effects of psychoactive substances. Our experiments confirmed that zebrafish larvae prefer blue color compared to yellow one [78]. Subsequently, we observed that incubation at the solution of 4-MMC in the less preferred color reversed initial preference, observed as more time spent in the yellow (initially less preferred) during the test. Our experiment confirmed that 4-MMC possesses reinforcing properties and these results correspond with our studies in rodent models [79]. Interestingly, incubation of zebrafish larvae at the solutions of MOFs blocked changes in color preference. Similar effects of MOFs were observed in the test of locomotor activity. The selected dose of 4-MMC (200 μM) increased locomotor activity. Most probably, the 4-MMC-induced increase in mobility is due to alterations in serotonergic and dopaminergic neurotransmission. This hyperlocomotion was reversed by incubation in MOFs solution. Thus, we may suggest that 4-MMC did not obtain the appropriate concentration to induce rewarding or locomotor effects.

The result of our study clearly indicates that the MOFs may be considered an efficient adsorbent of illicit drugs. The performed *in vivo* and *in vitro* experiments have clearly confirmed their superior efficiency in the removal of 4-MMC from the testing environment. The obtained results have demonstrated that the use of MOFs can be potentially considered efficient adsorbents during illicit drug overdose treatment.

Due to the significant high sorption efficiency of prepared materials for the removal of illicit drugs, we are currently planning *in vivo* experiments on higher organisms to develop effective doses of MOFs for the 4-MMC overdose treatment.

The practical aspects, like activity in the sorption or the exhibition of high biocompatibility, were regarded as the selection criterion, rather than the ligand similarity. Obviously, both studied materials have high surface area while possessing different channel systems which was reflected in the modeling studies. Based on our experimental and simulation studies, we have shown that the necessary condition for the efficient sorption was the presence of the π-π interactions which occurred in both MOF structures, while in NU-1000 the sorption was particularly efficient due to the presence of two kinds of channels. Therefore, NU-1000 for its high 4-MMC sorption capacity, durability, high biocompatibility, and cardioprotective properties may be considered as a prospective material for the removal of illicit drugs being, at the same time, safe for living organisms.

5. Outlook

The method of the removal of 4-MMC from liquid solutions presented in this study opens new strategies in one hand for the purification of water that is contaminated by drugs of abuse and the potential 4-MMC removal during the detoxification treatment. The obtained results clearly indicate the possible routes of the development of MOF as efficient 4-MMC adsorbents. The potential consideration of the application of Zr-MOFs to the removal of 4-MMC from liquid media should also consider raw materials and the possibility of large-scale synthesis. However, due to their well-known stability, durability, and reported numerous possible scale-up syntheses, NU-1000 and UiO-66 seem to be the most promising candidates for future applications.

Ethical approval

All experiments were conducted following the National Institute of Health Guidelines for the Care and Use of Laboratory Animals and to the European Community Council Directive for the Care and Use of Laboratory Animals of September 22, 2010 (2010/63/EU)—applies in Poland. For the experiment with larvae up to 5-dpf, agreement of the Local Ethical Commission is not required. After each experiment, larvae were immediately anesthetized and sacrificed with 15% tricaine. The experiment design was adhered to the ARRIVE guidelines for reporting animal research.

CRediT authorship contribution statement

Przemysław J. Jodłowski: Writing – review & editing, Writing – original draft, Validation, Supervision, Resources, Methodology, Investigation, Funding acquisition, Formal analysis, Data curation, Conceptualization. **Klaudia Dymek:** Investigation. **Grzegorz Kurowski:** Investigation. **Kornelia Hyjek:** Investigation. **Anna Boguszewska-**

Czubara: Writing – review & editing, Writing – original draft, Methodology, Investigation. **Barbara Budzyńska:** Writing – review & editing, Writing – original draft, Methodology, Investigation. **Anna Pajdak:** Writing – review & editing, Writing – original draft, Investigation. **Łukasz Kuterasiński:** Investigation. **Witold Piskorz:** Writing – review & editing, Writing – original draft, Methodology, Investigation. **Piotr Jeleń:** Investigation. **Maciej Sitarz:** Investigation.

Declaration of competing interest

The authors declare that they have no known competing financial interests or personal relationships that could have appeared to influence the work reported in this paper.

Data availability

Data will be made available on request.

Acknowledgements

The work was supported by the National Science Centre, Poland, under the research project "MOF-antidote": Novel detoxification materials based on metal-organic frameworks for drugs of abuse removal – synthesis, chemical characterization, toxicity and efficacy in *vivo* and *in vitro* studies", no. UMO-2021/43/B/NZ7/00827.

The *in vivo* studies were partially supported by Statutory Funds (140) from the Medical University of Lublin, Poland.

Appendix A. Supplementary data

Supplementary data to this article can be found online at https://doi.org/10.1016/j.micromeso.2023.112647.

References

[1] European monitoring Centre for drugs and drug addiction, europol, EU drug markets report, 2019, www.emcdda.europa.eu, 2019.
[2] European Monitoring Centre for Drugs Addiction and Europol, EU Drug Markets Report: In-Depth Analysis, EMCDDA–Europol Joint publications, Luxembourg, 2016.
[3] D. Aberg, D. Chaplin, C. Freeman, B. Paizs, C. Dunn, The environmental release and ecosystem risks of illicit drugs during Glastonbury Festival, Environ. Res. 204 (2022), 112061, https://doi.org/10.1016/j.envres.2021.112061.
[4] A.M. Sulej-Suchomska, A. Klupczynska, P. Dereziński, J. Matysiak, P. Przybyłowski, Z.J. Kokot, Urban wastewater analysis as an effective tool for monitoring illegal drugs, including new psychoactive substances, in the Eastern European region, Sci. Rep. 10 (2020) 81–87, https://doi.org/10.1038/s41598-020-61628-5.
[5] E.M. Mwenesongole, L. Gautam, S.W. Hall, J.W. Waterhouse, M.D. Cole, Simultaneous detection of controlled substances in waste water, Anal. Methods 5 (2013) 3248–3254, https://doi.org/10.1039/c3ay40655e.
[6] T. Gao, P. Du, Z. Xu, X. Li, Occurrence of new psychoactive substances in wastewater of major Chinese cities, Sci. Total Environ. 575 (2017) 963–969, https://doi.org/10.1016/j.scitotenv.2016.09.152.
[7] I. Haalck, P. Löffler, C. Baduel, K. Wiberg, L. Ahrens, F.Y. Lai, Mining chemical information in Swedish wastewaters for simultaneous assessment of population consumption, treatment efficiency and environmental discharge of illicit drugs, Sci. Rep. 11 (2021) 1–14, https://doi.org/10.1038/s41598-021-92915-4.
[8] F.P. Busardò, C. Kyriakou, S. Napoletano, E. Marinelli, S. Zaami, Mephedrone related fatalities: a review, Eur. Rev. Med. Pharmacol. Sci. 19 (2015) 3777–3790.
[9] J. Mead, A. Parrott, Mephedrone, MDMA, A comparative review, Brain Res. 1735 (2020), https://doi.org/10.1016/j.brainres.2020.146740.
[10] L. Anzillotti, L. Calò, A. Banchini, M.L. Schirripa, F. Marezza, R. Cecchi, Mephedrone and chemsex: a case report, Leg. Med. 42 (2020), https://doi.org/10.1016/j.legalmed.2019.101640.
[11] M. Aromatario, E. Bottoni, M. Santoni, C. Ciallella, New "Lethal highs": a case of a deadly cocktail of GHB and Mephedrone, Forensic Sci. Int. 223 (2012) 39–42, https://doi.org/10.1016/j.forsciint.2012.09.014.
[12] O.M. Yaghi, H. Li, Hydrothermal synthesis of a metal-organic framework containing large rectangular channels, J. Am. Chem. Soc. 117 (1995) 10401–10402, https://doi.org/10.1021/ja00146a033.
[13] S. Ahn, S.L. Nauert, C.T. Buru, M. Rimoldi, H. Choi, N.M. Schweitzer, J.T. Hupp, O. K. Farha, J.M. Notestein, Pushing the limits on metal–organic frameworks as a catalyst support: NU-1000 supported tungsten catalysts for o-xylene isomerization and disproportionation, J. Am. Chem. Soc. 140 (2018) 8535–8543, https://doi.org/10.1021/jacs.8b04059.
[14] L. Oar-Arteta, T. Wezendonk, X. Sun, F. Kapteijn, J. Gascon, Metal organic frameworks as precursors for the manufacture of advanced catalytic materials, Mater. Chem. Front. (2017) 1709–1745, https://doi.org/10.1039/C7QM00007C.
[15] C.D. Malonzo, S.M. Shaker, L. Ren, S.D. Prinslow, A.E. Platero-Prats, L. C. Gallington, J. Borycz, A.B. Thompson, T.C. Wang, O.K. Farha, J.T. Hupp, C. C. Lu, K.W. Chapman, J.C. Myers, R.L. Penn, L. Gagliardi, M. Tsapatsis, A. Stein, Thermal stabilization of metal-organic framework-derived single-site catalytic clusters through nanocasting, J. Am. Chem. Soc. 138 (2016) 2739–2748, https://doi.org/10.1021/jacs.5b12688.
[16] Y. He, F. Chen, B. Li, G. Qian, W. Zhou, B. Chen, Porous metal – organic frameworks for fuel storage, Coord. Chem. Rev. 373 (2018) 167–198, https://doi.org/10.1016/j.ccr.2017.10.002.
[17] J. Li, X. Wang, G. Zhao, C. Chen, Z. Chai, A. Alsaedi, T. Hayat, X. Wang, Metal-organic framework-based materials: superior adsorbents for the capture of toxic and radioactive metal ions, Chem. Soc. Rev. 47 (2018) 2322–2356, https://doi.org/10.1039/c7cs00543a.
[18] K. Dymek, G. Kurowski, Ł. Kuterasiński, R. Jędrzejczyk, M. Szumera, M. Sitarz, A. Pajdak, Ł. Kurach, A. Boguszewska-Czubara, P.J. Jodłowski, In search of effective UiO-66 metal–organic frameworks for artificial kidney application, ACS Appl. Mater. Interfaces 13 (2021) 45149–45160, https://doi.org/10.1021/acsami.1c05972.
[19] H.D. Lawson, S.P. Walton, C. Chan, Metal-organic frameworks for drug delivery: a design perspective, ACS Appl. Mater. Interfaces 13 (2021) 7004–7020, https://doi.org/10.1021/acsami.1c01089.
[20] I. Abánades Lázaro, C.J.R. Wells, R.S. Forgan, Multivariate modulation of the Zr MOF UiO-66 for defect-controlled combination anticancer drug delivery, Angew. Chem. Int. Ed. 59 (2020) 5211–5217, https://doi.org/10.1002/anie.201915848.
[21] Y. Li, J. Tang, L. He, Y. Liu, Y. Liu, C. Chen, Z. Tang, Core-Shell upconversion Nanoparticle@Metal-organic framework nanoprobes for luminescent/magnetic dual-mode targeted imaging, Adv. Mater. 27 (2015) 4075–4080, https://doi.org/10.1002/adma.201501779.
[22] X. Pan, L. Bai, H. Wang, Q. Wu, H. Wang, S. Liu, B. Xu, X. Shi, H. Liu, Metal–organic-framework-derived carbon nanostructure augmented sonodynamic cancer therapy, Adv. Mater. 30 (2018) 1–9, https://doi.org/10.1002/adma.201800180.
[23] B. Parmar, K.K. Bisht, G. Rajput, E. Suresh, Recent advances in metal-organic frameworks as adsorbent materials for hazardous dye molecules, Dalton Trans. 50 (2021) 3083–3108, https://doi.org/10.1039/d0dt03824e.
[24] Y.S. Seo, N.A. Khan, S.H. Jhung, Adsorptive removal of methylchlorophenoxypropionic acid from water with a metal-organic framework, Chem. Eng. J. 270 (2015) 22–27, https://doi.org/10.1016/j.cej.2015.02.007.
[25] M. Wagner, K.Y. Andrew Lin, W. Da Oh, G. Lisak, Metal-organic frameworks for pesticidal persistent organic pollutants detection and adsorption – a mini review, J. Hazard Mater. 413 (2021), 125325, https://doi.org/10.1016/j.jhazmat.2021.125325.
[26] Z. Hasan, S.H. Jhung, Removal of hazardous organics from water using metal-organic frameworks (MOFs): plausible mechanisms for selective adsorptions, J. Hazard Mater. 283 (2015) 329–339, https://doi.org/10.1016/j.jhazmat.2014.09.046.
[27] S.Y. Jiang, W.W. He, S.L. Li, Z.M. Su, Y.Q. Lan, Introduction of molecular building blocks to improve the stability of metal-organic frameworks for efficient mercury removal, Inorg. Chem. 57 (2018) 6118–6123, https://doi.org/10.1021/acs.inorgchem.8b00704.
[28] L. Esrafili, F.D. Firuzabadi, A. Morsali, M.L. Hu, Reuse of predesigned dual-functional metal organic frameworks (DF-MOFs) after heavy metal removal, J. Hazard Mater. 403 (2021), 123696, https://doi.org/10.1016/j.jhazmat.2020.123696.
[29] W. Liu, X. Shen, Y. Han, Z. Liu, W. Dai, A. Dutta, A. Kumar, J. Liu, Selective adsorption and removal of drug contaminants by using an extremely stable Cu(II)-based 3D metal-organic framework, Chemosphere 215 (2019) 524–531, https://doi.org/10.1016/j.chemosphere.2018.10.075.
[30] M.S. Samuel, K. Venkatesan Savunthari, N. Chandrasekar, R. Balaji, E. Selvarajan, Removal of environmental contaminants of emerging concern using metal–organic framework composite, Environ. Technol. Innov. 25 (2022), 102216, https://doi.org/10.1016/j.eti.2021.102216.
[31] F. Ahmadijokani, S. Tajahmadi, M. Rezakazemi, A.A. Sehat, H. Molavi, T. M. Aminabhavi, M. Arjmand, Aluminum-based metal-organic frameworks for adsorptive removal of anti-cancer (methotrexate) drug from aqueous solutions, J. Environ. Manag. 277 (2021), https://doi.org/10.1016/j.jenvman.2020.111448.
[32] T. Rasheed, M. Bilal, A.A. Hassan, F. Nabeel, R.N. Bharagava, L.F. Romanholo Ferreira, H.N. Tran, H.M.N. Iqbal, Environmental threatening concern and efficient removal of pharmaceutically active compounds using metal-organic frameworks as adsorbents, Environ. Res. 185 (2020), 109436, https://doi.org/10.1016/j.envres.2020.109436.
[33] S. Kato, K. Otake, H. Chen, I. Akpinar, C.T. Buru, T. Islamoglu, R.Q. Snurr, O. K. Farha, Zirconium-based metal–organic frameworks for the removal of protein-bound uremic toxin from human serum albumin, J. Am. Chem. Soc. 141 (2019) 2568–2576, https://doi.org/10.1021/jacs.8b12525.
[34] B.M. Jarai, Z. Stillman, L. Attia, G.E. Decker, E.D. Bloch, C.A. Fromen, Evaluating UiO-66 metal-organic framework nanoparticles as acid-sensitive carriers for pulmonary drug delivery applications, ACS Appl. Mater. Interfaces 12 (2020) 38989–39004, https://doi.org/10.1021/acsami.0c10900.

[35] A.J. Howarth, Y. Liu, P. Li, Z. Li, T.C. Wang, J.T. Hupp, O.K. Farha, Chemical, thermal and mechanical stabilities of metal-organic frameworks, Nat. Rev. Mater. 1 (2016) 1–15, https://doi.org/10.1038/natrevmats.2015.18.
[36] P.J. Jodłowski, K. Dymek, G. Kurowski, J. Jaśkowska, W. Bury, M. Pander, S. Wnorowska, K. Targowska-Duda, W. Piskorz, A. Wnorowski, A. Boguszewska-Czubara, Zirconium-based metal–organic frameworks as acriflavine cargos in the battle against Coronaviruses—A theoretical and experimental approach, ACS Appl. Mater. Interfaces 14 (2022) 28615–28627, https://doi.org/10.1021/acsami.2c06420.
[37] P.J. Jodłowski, G. Kurowski, Ł. Kuterasiński, M. Sitarz, P. Jeleń, J. Jaśkowska, A. Kołodziej, A. Pajdak, Z. Majka, A. Boguszewska-Czubara, Cracking the chloroquine conundrum: the application of defective UiO-66 metal–organic framework materials to prevent the onset of heart defects—in vivo and in vitro, ACS Appl. Mater. Interfaces 13 (2021) 312–323, https://doi.org/10.1021/acsami.0c21508.
[38] Z. Xu, G. Zhao, L. Ullah, M. Wang, A. Wang, Y. Zhang, S. Zhang, Acidic ionic liquid based UiO-67 type MOFs: a stable and efficient heterogeneous catalyst for esterification, RSC Adv. 8 (2018) 10009–10016, https://doi.org/10.1039/c8ra01119b.
[39] D. Yang, S.O. Odoh, T.C. Wang, O.K. Farha, J.T. Hupp, C.J. Cramer, L. Gagliardi, B. C. Gates, Metal-organic framework nodes as nearly ideal supports for molecular catalysts: NU-1000- and UiO-66-supported iridium complexes, J. Am. Chem. Soc. 137 (2015) 7391–7396, https://doi.org/10.1021/jacs.5b02956.
[40] G.C. Shearer, S. Chavan, J. Ethiraj, J.G. Vitillo, S. Svelle, U. Olsbye, C. Lamberti, S. Bordiga, K.P. Lillerud, Tuned to perfection: ironing out the defects in metal-organic framework UiO-66, Chem. Mater. 26 (2014) 4068–4071, https://doi.org/10.1021/cm501859p.
[41] S. Kato, Zirconium-Based Metal–Organic Frameworks for the Removal of Protein-Bound Uremic Toxin from Human Serum Albumin, 2015, pp. 1–27.
[42] T. Kokubo, H. Takadama, How useful is SBF in predicting in vivo bone bioactivity? Biomaterials 27 (2006) 2907–2915, https://doi.org/10.1016/j.biomaterials.2006.01.017.
[43] Y. Wang, Measurements and modeling of water adsorption isotherms of zeolite linde-type A crystals, Ind. Eng. Chem. Res. 59 (2020) 8304–8314, https://doi.org/10.1021/acs.iecr.9b06891.
[44] G. Kresse, J. Furthmüller, Efficiency of ab-initio total energy calculations for metals and semiconductors using a plane-wave basis set, Comput. Mater. Sci. 6 (1996) 15–50, https://doi.org/10.1016/0927-0256(96)00008-0.
[45] G. Kresse, J. Hafner, Ab initio molecular dynamics for open-shell transition metals, Phys. Rev. B 48 (1993) 13115–13118, https://doi.org/10.1103/PhysRevB.48.13115.
[46] E. Kozioł, K. Skalicka-Woźniak, A. Michalak, K. Kaszubska, B. Budzyńska, Xanthotoxin reverses Parkinson's disease-like symptoms in zebrafish larvae and mice models: a comparative study, Pharmacol. Rep. 73 (2021) 122–129, https://doi.org/10.1007/s43440-020-00136-9.
[47] OECD, Test No. 236: Fish Embryo Acute Toxicity (FET) Test, 2013, https://doi.org/10.1787/9789264203709-en.
[48] T.C. Wang, N.A. Vermeulen, I.S. Kim, A.B.F. Martinson, J. Fraser Stoddart, J. T. Hupp, O.K. Farha, Scalable synthesis and post-modification of a mesoporous metal-organic framework called NU-1000, Nat. Protoc. 11 (2016) 149–162, https://doi.org/10.1038/nprot.2016.001.
[49] G.C. Shearer, S. Chavan, S. Bordiga, S. Svelle, U. Olsbye, K.P. Lillerud, Defect engineering: tuning the porosity and composition of the metal-organic framework UiO-66 via modulated synthesis, Chem. Mater. 28 (2016) 3749–3761, https://doi.org/10.1021/acs.chemmater.6b00602.
[50] S. Brunauer, The Adsorption of Gases and Vapors, Princeton University press, Princeton, 1943.
[51] I. Langmuir, The adsorption of gases on plane surfaces of glass, mica and platinum, J. Am. Chem. Soc. 40 (1918) 1361–1403, https://doi.org/10.1021/ja02242a004.
[52] P. Deria, J.E. Mondloch, E. Tylianakis, P. Ghosh, W. Bury, R.Q. Snurr, J.T. Hupp, O. K. Farha, Perfluoroalkane functionalization of NU-1000 via solvent-assisted ligand incorporation : synthesis and CO2 adsorption studies, J. Am. Chem. Soc. 135 (2013) 16801–16804.
[53] E.Y. Santali, A.K. Cadogan, N.N. Daeid, K.A. Savage, O.B. Sutcliffe, Synthesis, full chemical characterisation and development of validated methods for the quantification of (±)-4'-methylmethcathinone (mephedrone): a new "legal high,", J. Pharm. Biomed. Anal. 56 (2011) 246–255, https://doi.org/10.1016/j.jpba.2011.05.022.
[54] J.H. Cavka, S. Jakobsen, U. Olsbye, N. Guillou, C. Lamberti, S. Bordiga, K. P. Lillerud, A new zirconium inorganic building brick forming metal organic frameworks with exceptional stability, J. Am. Chem. Soc. 130 (2008) 13850–13851, https://doi.org/10.1021/ja8057953.
[55] K.I. Otake, Y. Cui, C.T. Buru, Z. Li, J.T. Hupp, O.K. Farha, Single-atom-based vanadium oxide catalysts supported on metal-organic frameworks: selective alcohol oxidation and structure-activity relationship, J. Am. Chem. Soc. 140 (2018) 8652–8656, https://doi.org/10.1021/jacs.8b05107.
[56] B.T. Yost, B. Gibbons, A. Wilson, A.J. Morris, L.E. McNeil, Vibrational spectroscopy investigation of defects in Zr- and Hf-UiO-66, RSC Adv. 12 (2022) 22440–22447, https://doi.org/10.1039/d2ra03131k.
[57] S. Mabbott, E. Correa, D.P. Cowcher, J.W. Allwood, R. Goodacre, Optimization of parameters for the quantitative surface-enhanced Raman scattering detection of mephedrone using a fractional factorial design and a portable Raman spectrometer, Anal. Chem. 85 (2013) 923–931, https://doi.org/10.1021/ac302542r.
[58] K. Tsujikawa, T. Mikuma, K. Kuwayama, H. Miyaguchi, T. Kanamori, Y.T. Iwata, H. Inoue, Degradation pathways of 4-methylmethcathinone in alkaline solution and stability of methcathinone analogs in various pH solutions, Forensic Sci. Int. 220 (2012) 103–110, https://doi.org/10.1016/j.forsciint.2012.02.005.
[59] United Nations Office on Drugs and Crime, Recommended Methods for the Identification and Analysis of Synthetic Cathinones in Seized Materials, UNITED NATIONS, Vienna, 2020.
[60] A. Camilleri, M.R. Johnston, M. Brennan, S. Davis, D.G.E. Caldicott, Chemical analysis of four capsules containing the controlled substance analogues 4-methylmethcathinone, 2-fluoromethamphetamine, α-phthalimidopropiophenone and N-ethylcathinone, Forensic Sci. Int. 197 (2010) 59–66, https://doi.org/10.1016/j.forsciint.2009.12.048.
[61] N. Sun, D. Qi, Y. Jin, H. Wang, C. Wang, C. Qu, J. Liu, Y. Jin, W. Zhang, J. Jiang, Porous pyrene organic cage with unusual absorption bathochromic-shift enables visible light photocatalysis, CCS Chem 4 (2022) 2588–2596, https://doi.org/10.31635/ccschem.021.202101202.
[62] A. Schaate, P. Roy, A. Godt, J. Lippke, F. Waltz, M. Wiebcke, P. Behrens, Modulated synthesis of Zr-based metal-organic frameworks: from nano to single crystals, Chem. Eur J. 17 (2011) 6643–6651, https://doi.org/10.1002/chem.201003211.
[63] S. Höhn, K. Zheng, S. Romeis, M. Brehl, W. Peukert, D. de Ligny, S. Virtanen, A. R. Boccaccini, Effects of medium pH and preconditioning treatment on protein adsorption on 45S5 bioactive glass surfaces, Adv. Mater. Interfac. 7 (2020), https://doi.org/10.1002/admi.202000420.
[64] W. Liu, Z. Yan, Z. Zhang, Y. Zhang, G. Cai, Z. Li, Bioactive and anti-corrosive bio-MOF-1 coating on magnesium alloy for bone repair application, J. Alloys Compd. 788 (2019) 705–711, https://doi.org/10.1016/j.jallcom.2019.02.281.
[65] Y. Feng, Q. Chen, M. Jiang, J. Yao, Tailoring the properties of UiO-66 through defect engineering: a review, Ind. Eng. Chem. Res. 58 (2019) 17646–17659, https://doi.org/10.1021/acs.iecr.9b03188.
[66] Z. Fang, B. Bueken, D.E. De Vos, R.A. Fischer, Defect-engineered metal-organic frameworks, Angew. Chem. Int. Ed. 54 (2015) 7234–7254, https://doi.org/10.1002/anie.201411540.
[67] S. Øien, D. Wragg, H. Reinsch, S. Svelle, S. Bordiga, C. Lamberti, K.P. Lillerud, Detailed structure analysis of atomic positions and defects in zirconium metal-organic frameworks, Cryst. Growth Des. 14 (2014) 5370–5372, https://doi.org/10.1021/cg501386j.
[68] M.J. Cliffe, E. Castillo-Martínez, Y. Wu, J. Lee, A.C. Forse, F.C.N. Firth, P. Z. Moghadam, D. Fairen-Jimenez, M.W. Gaultois, J.A. Hill, O.V. Magdysyuk, B. Slater, A.L. Goodwin, C.P. Grey, Metal-organic nanosheets formed via defect-mediated transformation of a hafnium metal-organic framework, J. Am. Chem. Soc. 139 (2017) 5397–5404, https://doi.org/10.1021/jacs.7b00106.
[69] C. Koschnick, R. Stäglich, T. Scholz, M.W. Terban, A. von Mankowski, G. Savasci, F. Binder, A. Schökel, M. Etter, J. Nuss, R. Siegel, L.S. Germann, C. Ochsenfeld, R. E. Dinnebier, J. Senker, B.V. Lotsch, Understanding disorder and linker deficiency in porphyrinic zirconium-based metal–organic frameworks by resolving the Zr8O6 cluster conundrum in PCN-221, Nat. Commun. 12 (2021) 1–9, https://doi.org/10.1038/s41467-021-23348-w.
[70] T. Zellner, D. Prasa, E. Färber, P. Hoffmann-Walbeck, D. Genser, F. Eyer, The use of activated charcoal to treat intoxications, Dtsch. Arztebl. Int. 116 (2019) 311–317, https://doi.org/10.3238/arztebl.2019.0311.
[71] G.S. Winder, N. Stern, A. Hosanagar, Are "Bath Salts" the next generation of stimulant abuse? J. Subst. Abuse Treat. 44 (2013) 42–45, https://doi.org/10.1016/j.jsat.2012.02.003.
[72] E. Dreosti, G. Lopes, A.R. Kampff, S.W. Wilson, Development of social behavior in young zebrafish, Front. Neural Circ. 9 (2015) 1–9, https://doi.org/10.3389/fncir.2015.00039.
[73] V.B. Maphanga, K. Skalicka-Wozniak, B. Budzynska, A. Skiba, W. Chen, C. Agoni, G.M. Enslin, A.M. Viljoen, Mesembryanthemum tortuosum L. alkaloids modify anxiety-like behaviour in a zebrafish model, J. Ethnopharmacol. 290 (2022), 115068, https://doi.org/10.1016/j.jep.2022.115068.
[74] A.C. Miller, L.H. Voelker, A.N. Shah, C.B. Moens, Chemical Synapse Formation 25 (2016) 16–28, https://doi.org/10.1016/j.cub.2014.10.071.Neurobeachin.
[75] M.E. Suryanto, G. Audira, B. Uapipatanakul, A. Hussain, F. Saputra, P. Siregar, K.H. C. Chen, C. Der Hsiao, Antidepressant screening demonstrated non-monotonic responses to amitriptyline, amoxapine and sertraline in locomotor activity assay in larval zebrafish, Cells 10 (2021), https://doi.org/10.3390/cells10040738.
[76] A.S. Glass, R. Dahm, The zebrafish as a model organism for eye development, Ophthalmic Res. 36 (2004) 4–24, https://doi.org/10.1159/000076105.
[77] P. Goldsmith, W.A. Harris, The zebrafish as a tool for understanding the biology of visual disorders, Semin. Cell Dev. Biol. 14 (2003) 11–18, https://doi.org/10.1016/S1084-9521(02)00167-2.
[78] J.S. Park, J.H. Ryu, T.I. Choi, Y.K. Bae, S. Lee, H.J. Kang, C.H. Kim, Innate color preference of zebrafish and its use in behavioral analyses, Mol. Cell. 39 (2016) 750–755, https://doi.org/10.14348/molcells.2016.0173.
[79] O. Wronikowska, M. Zykubek, Ł. Kurach, A. Michalak, A. Boguszewska-Czubara, B. Budzyńska, Vulnerability factors for mephedrone-induced conditioned place preference in rats—the impact of sex differences, social-conditioning and stress, Psychopharmacology (Berl) 238 (2021) 2947–2961, https://doi.org/10.1007/s00213-021-05910-y.
[80] K. Styszko, A. Dudarska, D. Zuba, The presence of stimulant drugs in wastewater from krakow (Poland): a snapshot, Bull. Environ. Contam. Toxicol. 97 (2016) 310–315, https://doi.org/10.1007/s00128-016-1869-5.
[81] P. Hu, C. Guo, Y. Zhang, J. Lv, Y. Zhang, J. Xu, Occurrence, distribution and risk assessment of abused drugs and their metabolites in a typical urban river in north China, Front, Environ. Sci. Eng. 13 (2019), https://doi.org/10.1007/s11783-019-1140-5.
[82] S. Castiglioni, A. Borsotti, I. Senta, E. Zuccato, Wastewater analysis to monitor spatial and temporal patterns of use of two synthetic recreational drugs, Ketamine

and Mephedrone, in Italy, Environ. Sci. Technol. 49 (2015) 5563–5570, https://doi.org/10.1021/es5060429.